



High-mobility carriers and superconductivity at the SrNbO₃-SrTiO₃ interfaceHaoran Wei ^{1,2,*}, Shengru Chen,^{1,2,*} Yuting Zou,^{1,2} Yuxin Wang,^{1,2} Meng Yang,^{1,2} Qinghua Zhang,^{1,2,5}
Ke Zou,³ Lin Gu,⁴ Kun Jiang,^{1,2,5} Er-Jia Guo,^{1,2,5,†} and Zhi Gang Cheng ^{1,2,5,‡}¹*Beijing National Laboratory for Condensed Matter Physics, Institute of physics, Chinese Academy of Sciences, Beijing, 100190, China*²*School of Physics, University of Chinese Academy of Sciences, Beijing, 100049, China*³*Department of Physics & Astronomy and Quantum Matter Institute, University of British Columbia, Vancouver, Canada, BC V6T 1Z1*⁴*National Center for Electron Microscopy in Beijing and School of Materials Science and Engineering, Tsinghua University, Beijing 100084, China*⁵*Songshan Lake Materials Laboratory, Dongguan, Guangdong, 523808, China*

(Received 3 February 2023; revised 25 October 2023; accepted 10 April 2024; published 2 May 2024)

Interfaces between transition-metal oxides can host two-dimensional electron gases (2DEGs) that exhibit intriguing quantum phenomena. The interfacial 2DEG system has attracted significant attention due to its versatile properties and tunability. In this study, we present the discovery of a high-mobility 2DEG characterized by well-developed Shubnikov-de Haas oscillations, alongside superconductivity at temperatures below 230 mK, in a heterostructure comprising bulk-metallic SrNbO₃ on SrTiO₃. The 2DEG is featured with extremely low carrier density for the quantum oscillations, and the superconductivity with two-step behaviors in various transport properties. Both the 2DEG and the superconductivity exhibit a common dependence on the thickness of the SrNbO₃ layer. The dependence underscores the crucial role of epitaxial strain within the metallic layer on these two phenomena. Our findings introduce a novel platform for investigating interfacial high-mobility 2DEGs coexisting with superconductivity, with the bulk-metallic components of SrNbO₃ playing a pivotal role in these heterostructures.

DOI: [10.1103/PhysRevB.109.205404](https://doi.org/10.1103/PhysRevB.109.205404)

Interfaces between transition-metal oxides (TMOs) have attracted remarkable interests because of their potential in hosting two-dimensional electron gases (2DEGs) with distinct band structures and exotic properties. The first realization of 2DEG at the interface between LaAlO₃ (LAO) and SrTiO₃ (STO) [1] provides a ground-breaking platform to demonstrate exotic quantum phenomena [2–10], among which superconductivity attracts tremendous attention because of its importance in fundamental sciences and practical applications [11,12]. Recently, substitution of STO by KTaO₃ (KTO) is expected to introduce stronger topological nature because KTO's spin-orbit coupling (SOC) strength is more than 20 times larger [13]. Interfacial superconductivity has been realized for heterostructures of EuO/KTO and LAO/KTO till now with specific crystalline orientations [14–20].

2DEGs usually reside on one side of the TMO heterostructures within STO or KTO. The 2DEG at LAO/STO heterostructures is thought to be formed via charge transfer from LAO to STO due to the discontinuity of polarity at interfaces [21]. Nevertheless, the general formation mechanism of the electron systems within TMO heterostructures is obscure. Besides interfacial charge transfer, oxygen vacancies are also possible sources of extra charge carriers [22] while their existence is unstable for quantitative controls or analyses. Intermixing of atoms have also been observed in systems

that create 2DEGs at the interface [23]. On the other hand, introducing exotic properties such as topological band structures and magnetic orders is usually realized by engineering the adjacent overlayer, but not always convenient. Proximity effect, the major route for such engineering, is usually limited by multiple factors such as robustness of the property, quality of interfaces, etc. Novel methods of constructing and engineering interfacial superconductivity is therefore needed.

The difficulty mentioned above may be relieved by depositing a metallic overlayer. With large charge density and affinity to electrons, the metallic layer could either build stronger interactions with the 2DEGs in STO or KTO via proximity effect, or even make the 2DEGs cross the interface and reside in the overlayer. As a metallic perovskite in bulk phase, SrNbO₃ (SNO) possesses Nb's 4d orbitals and is expected to integrate the electron system with both strong correlations and large SOC. It is an appropriate candidate to realize a 2DEG near the interface and to explore exotic properties, including unconventional or topological superconductivity [24–26].

Here, we report on the observation of the coexistence of superconductivity and Shubnikov-de Haas (SdH) oscillations in SNO/STO heterostructures. The superconducting transition temperature varies between 150 and 230 mK, being dependent on the thickness of the SNO layer. A high-mobility electron system is inferred to exist by the SdH oscillations. Notably, its carrier density is 4 ~ 5 orders of magnitude smaller than that of all itinerant charge carriers, which is suggestive of its unique formation mechanism. Both the superconductivity and SdH oscillations exhibit similar dependence on the thickness of the SNO layer, implying their origins near the interface at

*These two authors contributed equally.

†ejguo@iphy.ac.cn

‡zgcheng@iphy.ac.cn

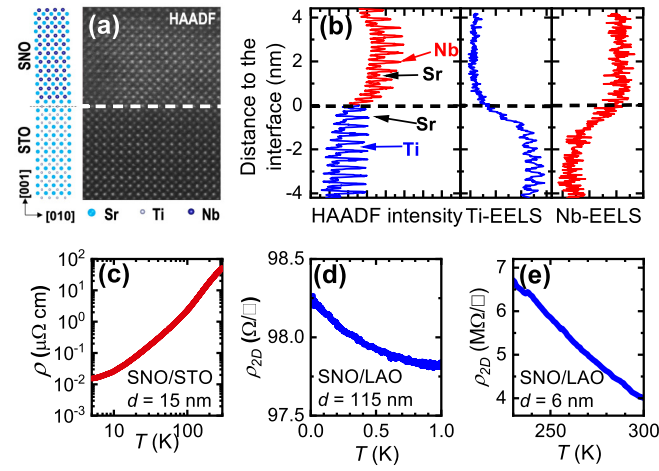


FIG. 1. (a) STEM picture of the SNO/STO interface looking along the [100] direction. (b) Characterizations of chemical intermixing at the interface by HAADF and EELS intensities. (c) Temperature dependence of a SNO/STO heterostructure with $d = 15$ nm from 300 to 4 K. Temperature dependencies of SNO/LAO heterostructures are shown in (d) and (e) with $d = 115$ and 6 nm, respectively.

the SNO side. It is by far unclear whether these two stem from the same electron system.

High-quality SNO films were deposited on STO substrates with (001) orientation and TiO_2 -terminated surface by pulsed laser deposition (PLD) technique. An atomically sharp interface could be confirmed by high-angle annular dark-field scanning transmission electron microscopy (HAADF-STEM) [see Fig. 1(a)]. With the lattice constants being 3.905 \AA for STO and 4.023 \AA for SNO, the substrate exerts an in-plane biaxially compressive strain $\epsilon = -3.02\%$. Electron energy loss spectroscopy (EELS) [see Fig. 1(b)] displays the distributions of Ti and Nb elements and suggests a sharp transition across the interface. The chemical intermixing could not be detected within the measurement resolution (about two unit cells) and the HAADF intensity near the interface clearly exhibits periodic arrangement of SrO , NbO_2 , and TiO_2 planes. Both the HAADF and EELS results convincingly confirm high crystalline quality of the oxides and the sharpness of the interface. A series of SNO/STO heterostructures were prepared with the thickness of SNO layer $d = 4, 6, 15, 37, 75, 150$ nm. All samples are square shaped with dimensions of $5 \times 5 \text{ mm}^2$.

Electric transport measurements were conducted using the van der Pauw (vdP) method from room to ultralow temperatures (~ 20 mK). A typical residual resistance ratio (RRR) is as high as ~ 3000 for all samples [Fig. 1(c)], confirming the high crystallinity of SNO films. Superconductivity was observed for the samples with $d \geq 6$ nm [see Fig. 2(a)]. The transition temperature (T_c), determined by the onsets of resistance drops, monotonically increases with d from 150 to 230 mK. The 37 nm sample exhibits a two-step transition during the resistance drop at around 150 mK.

For control experiments, we prepared another two heterostructures by depositing SNO ($d = 6$ and 115 nm, respectively) on LaAlO_3 (LAO) substrates. The 6 nm film is insulating with sheet resistivity on the order of $\text{M}\Omega$ [see

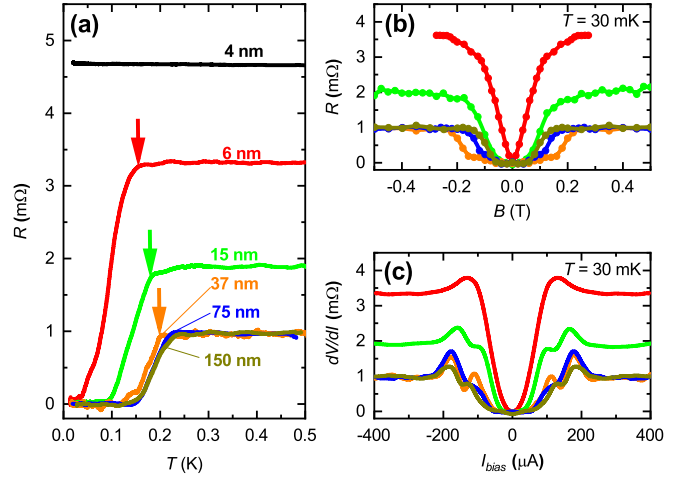


FIG. 2. (a) Temperature dependence of resistances for all the SNO/STO samples. The arrows label the superconducting transition temperatures T_c . (b) Resistances as magnetic field varies between ± 0.5 T at 30 mK. (c) Differential resistances (dV/dI) as I_{bias} varies between $\pm 400 \mu\text{A}$ at 30 mK.

Fig. 1(e)]. The transition from being metallic to insulating is due to the strain exerted by the substrate. On the other hand, it provides further confirmation about the high crystalline quality for the deposited SNO film. The 115 nm sample, although recovering the metallicity at higher temperatures because of strain relaxation, still exhibits a mild insulating behavior below 1.0 K. More importantly, no superconductivity was observed down to 20 mK [see Fig. 1(d)]. It convinces that the observed superconductivity is unique to the specific combination of SNO and STO and does not stem from the relaxed bulk SNO.

We further characterize the superconductivity by varying magnetic field (B) and bias current (I_{bias}). Both $R - B$ and $dV/dI - I_{\text{bias}}$ curves shown in Figs. 2(b) and 2(c) evolve from “V” to “U” shape as d increases, suggesting the strengthening of superconductivity. Again, a two-step behavior is discernible in the R_B curve for the 37 nm sample, and more obvious in the $dV/dI - I_{\text{bias}}$ curves for all except the 6 nm sample. Figure 3(b) summarizes the thickness dependence of two-dimensional conductivity before superconducting transition (σ_{2D}), T_c , critical current (I_c), and critical field ($\mu_0 H_c$). Here

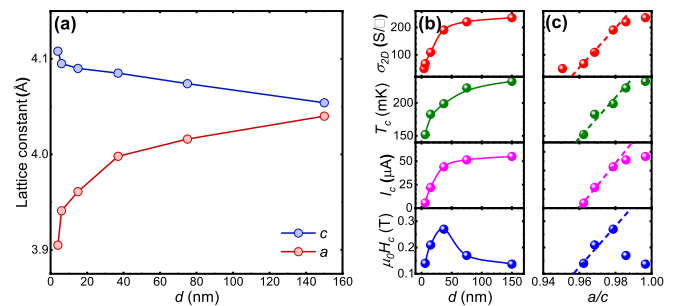


FIG. 3. (a) In-plane (a) and out-of-plane (c) lattice constants as functions of SNO thickness extracted by XRD measurements. (b) Thickness dependence of σ_{2D} , T_c , I_c , and H_c . (c) Dependence on a/c for the same data shown in panel (b). The dashed lines indicate linear dependencies.

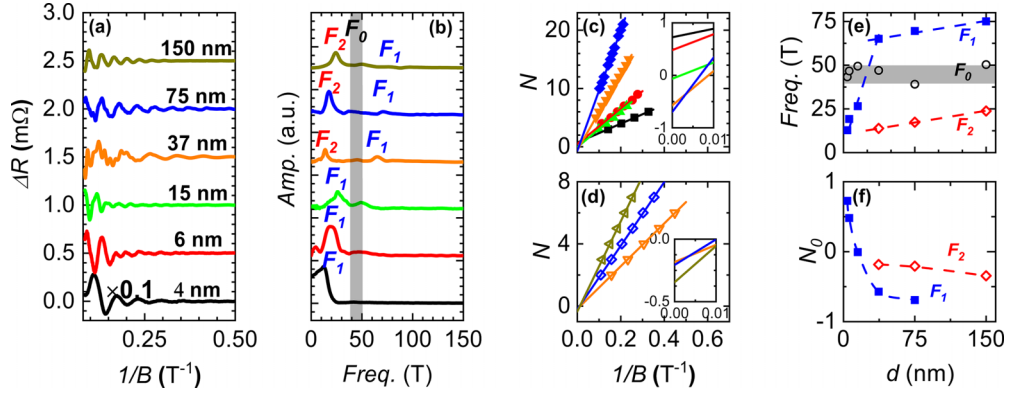


FIG. 4. (a) SdH oscillations and (b) fast Fourier transformation (FFT) spectra for all samples. (c) and (d) are Landau fan diagrams for F_1 and F_2 oscillations, respectively. The insets show zoom-in views of intercepts of each diagram. (e) Thickness dependence of identified frequencies. The oscillations are dominated by F_1 for $d < 15$ nm and by F_2 for $d > 37$ nm, while interference of two appears for $d = 37$ nm [shown in panel (a)]. The shaded belt highlights the weak peak of F_0 . (f) N_0 for F_1 and F_2 oscillations for various d .

$\mu_0 H_c$ is determined by the field at which resistances drop to 90% of the normal state values, and I_c is determined by the onsets of sudden increases of dV/dI . All the parameters rapidly increase before d reaches 37 nm. For larger d , the first three universally switch to a much slower increasing rate, but $\mu_0 H_c$ significantly decreases.

The thickness dependence is likely associated with the relaxation of in-plane biaxial strain exerted by the substrates. Compression leads to smaller in-plane lattice constant (a) and larger out-of-plane lattice constant (c). As d increases, the influence of the substrate fades away, and a and c gradually merge. They were characterized by x-ray diffraction (XRD) measurements for each sample [see Fig. 3(a)], and impressively exhibit similar thickness dependence as the superconductivity—rapid change for $d < 37$ nm and mild evolution for larger d . Strain relaxation can be seen in further details by reciprocal space mapping (RSM) measurements (see Fig. S2 in the Supplemental Material [27]). Both XRD and RSM data prove that most of the strain is relaxed within 37 nm from the interface where a large strain gradient exists. The strong effect of the strain gradient on superconductivity can be seen in Fig. 3(c).

Strain can have an impact on the carrier density and band structure [31]. For perovskite compounds, the split between t_{2g} and e_g bands is caused by crystal field and is thus sensitive to strains; orbital energies within each band also differ when spatial symmetry is broken, leading to further lift of degeneracy. The evolution under strain may lead to reconstruction of band structure. For instance, a Dirac point in SNO is predicted to emerge not far from Fermi level when compressive strains and rotations of NbO_6 tetrahedrals are considered [25].

To exploit the effects of epitaxial strain modulation on band structures, we conducted magnetoresistance measurements for all samples. Similar as the previous study [32], large linear magnetoresistances (LMR) were observed (see Fig. S4 of the Supplemental Material [27]). In addition, SdH oscillations were observed superimposed to the LMR. The oscillations are periodic in $1/B$, and composed of two major frequencies [Figs. 4(a) and 4(b)]. One (F_1) rapidly shifts upwards for $4 \text{ nm} < d < 37 \text{ nm}$, and switches to a slower increasing rate for larger d ; another (F_2) is only visible for $d > 37 \text{ nm}$ and

mildly increases [see Fig. 4(e)]. The thickness dependence of F_1 agrees with that for the strain. The coincidence not only unveils the strong modulation of strain on band structure, but also implies the correlation with strain for both the superconductivity and the quantum oscillations. Another weak spectral peak (labeled as F_0) exists between 38 and 50 T with no obvious dependence on d . Its obscurity might be associated with low mobility of the corresponding band.

Landau-fan diagrams for F_1 and F_2 are plotted in Figs. 4(c) and 4(d). The integer indices of Landau levels are marked at the minima of the oscillating component ΔR because $\rho_{xy} \gg \rho_{xx}$ (see Fig. S5 in the Supplemental Material [27]). According to the Lifshitz-Onsager quantization rule, $S_F \cdot (h/eB) = 2\pi(N + N_0) = 2\pi(N + 1/2 + \gamma)$, where S_F is the Fermi surface area, h the Planck's constant, and e the electron charge. Here $N_0 = 1/2 + \gamma$ is the intercept of Landau-fan diagram and γ is associated with dimensionality and Berry phase. We note that N_0 of the F_1 Landau-fan diagram continuously evolves as d increases [see Fig. 4(f)], exhibiting similar thickness dependence.

The metallicity of bulk SNO and possible oxygen vacancies within the STO substrates introduce complexity to analyses. We therefore aim to estimate their charge carrier densities that contribute to the transport process. Figure 5(a)

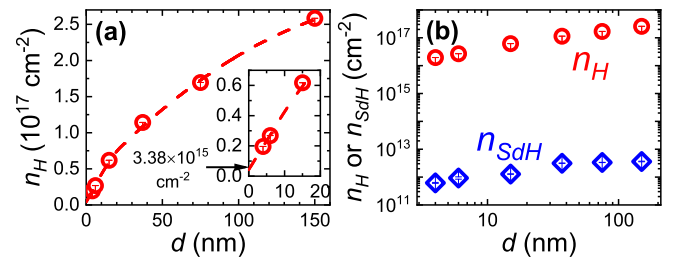


FIG. 5. (a) Carrier densities extracted by Hall measurements. The dashed line is a guide to the eye. Inset: zoom-in view for $d < 20$ nm. The intercept $n_{H0} = 3.38 \times 10^{15} \text{ cm}^{-2}$ at $d = 0$ is a residue density associated with the doped STO. (b) Comparison of carrier densities extracted from Hall measurements and the SdH oscillations. The estimated error bars are smaller than the symbol size.

plots the two-dimensional carrier densities as a function of SNO thickness. The densities n_H are determined by Hall measurements, which include the contributions from all itinerant charges. The extrapolation to the $d = 0$ limits, which excludes the contribution from the SNO layer, gives a finite value of $n_{H0} = 3.38 \times 10^{15} \text{ cm}^{-2}$. This is in consistency with other STO-based heterostructures with insulating overlayers [1]. Given the small uncertainties of n_H , the estimation of n_{H0} should be sufficiently precise [see the inset of Fig. 5(a)]. On the other hand, the densities of the high-mobility electron system, inferred by the SdH oscillations, are given by $n_{SdH} = (2e/h)F_1 = (0.6 \sim 3.6) \times 10^{12} \text{ cm}^{-2}$ where the spin degeneracy of two has been taken into account. It is 3 ~ 4 orders of magnitude smaller than n_{H0} [see Fig. 5(b)], suggesting that n_{H0} is mainly contributed by the charge carriers within the STO substrates due to oxygen vacancies doped during the sample growth [33–36].

The high-mobility electron system is featured with some specialties which imply its possible unique formation mechanism. First, It should not reside in the bulk metallic SNO because the mobility and phase coherence will be easily destroyed by itinerant charges. Second, given the 2DEGs in LAO/STO heterostructures may also exhibit SdH oscillations [37–42], it seems that oxygen vacancies could be one possible mechanism for the high-mobility electrons in our samples. However, one should note that although there is constantly a difference between n_{SdH} and n_H in these studies ($n_{H0}/n_{SdH} = 3 \sim 5$ [41]), the ratio for the SNO/STO samples $n_{H0}/n_{SdH} > 10^3$ is 2 ~ 3 orders of magnitude larger. Furthermore, the lowest $n_{SdH} = 0.6 \times 10^{12} \text{ cm}^{-2}$ is lower than that for two-dimensional LAO/STO heterostructures, while compatible a one-dimensional counterpart [42]. On the other hand, the dependence of $n_{SdH} (\propto F_1)$ on d still suggests its close relation with the metallic SNO layer. One possible mechanism is that charges transfer from bulk SNO toward the interface under a strain gradient. This agrees with the density-functional-theory (DFT) calculations which demonstrate a charge accumulation at the interface (see Fig. S7 in the Supplemental Material [27]). We emphasize that this mechanism is completely different from the transfer due to interfacial polar catastrophe.

STO can indeed exhibit superconductivity by doping oxygen vacancies or intermixing Nb [43]. The optimal dosage gives a carrier density between 10^{17} and 10^{20} cm^{-3} [33,34,44]. For our case, the carrier density—if converted from n_{H0} for a typical thickness less than 100 nm—is beyond this range, otherwise it requires a doped layer thicker than 340 nm to exhibit superconductivity. Such a thickness, while not completely ruling out the possibility, is extremely unlikely. Moreover, the two-step behaviors exhibited by the SNO/STO superconductivity, including $R - T$, $R - B$, $dV/dI - I_{\text{bias}}$ curves (shown in Fig. 2) and the temperature dependence of critical field (shown in Fig. S3 in the Supplemental Material [27]), have not been observed for LAO/STO heterostructures. Alternatively, the thickness dependence of

superconductivity gives a strong indication that it is closely related with the SNO layer, although the contribution of superconductivity in the doped STO cannot be ruled out conclusively. Considering the absence of superconductivity has been verified by the SNO(115 nm)/LAO heterostructure, it should originate from the interface or the strained SNO. So far, there is no convincing evidence to attribute both the superconductivity and the SdH oscillations to the same electron system, although their correlations with the strain can be confirmed by the thickness dependence in common. The statement is strengthened further by the simultaneous appearance of the abnormal suppression of $\mu_0 H_c$ [see Fig. 3(c)] and the F_2 oscillations for $d > 37 \text{ nm}$. A detailed investigation on the suppression shows that the linear temperature dependence of $\mu_0 H_c$ breaks into two sections (see Fig. S3 in the Supplemental Material [27]). The nature of multiband structure has been confirmed for SNO both by angle-resolved photoemission spectroscopy (ARPES) experiments and DFT calculations [24]. With a larger SNO thickness, carrier density increases to a threshold and starts to fill the higher band, thus introducing certain mechanisms to suppress superconducting order parameters.

In summary, we have fabricated a series of heterostructures composed of metallic SrNbO₃ and insulating SrTiO₃, and observed superconductivity coexisting with Shubnikov-de Haas oscillations. The superconducting transition temperature varies between 150 and 230 mK, and the SdH oscillations confirm the existence of high-mobility 2DEG with a density in the range of $(0.6 \sim 3.6) \times 10^{12} \text{ cm}^{-2}$. Both phenomena exhibit similar dependence on the thickness of the SNO layer. Careful analyses have been performed to determine that both phenomena are located in the strained region of SNO near the interface, distinguished from previous reports on LAO/STO heterostructures. The formation of the 2DEG is likely driven by a mechanism of charge transfer from the bulk metallic SNO toward the interface triggered by strain gradient. The superconductivity is also closely related with the strain, although whether it originates from the high-mobility 2DEG is unclear. Our results convince that heterostructures of metallic and insulating TMOs is an appealing platform for the study of interfacial emergent phenomena.

We thank Qihong Chen for fruitful discussions. This work is supported by the National Key R&D Program of China Grant (Grants No. 2021YFA1401902 and No. 2020YFA0309100), the National Natural Science Foundation of China (NSFC) (No. T2325026, 11874403, 11974390, 12174428), the Key Research Program of Frontier Sciences, CAS, (Grant No. ZDBS-LY-SLH0010), the Beijing Natural Science Foundation (Grant No. JQ21002), the Guangdong-Hong Kong-Macao Joint Laboratory for Neutron Scattering Science and Technology, and the Strategic Priority Research Program (B) of the Chinese Academy of Sciences (Grant No. XDB33030200).

- [1] A. Ohtomo and H. Y. Hwang, A high-mobility electron gas at the $\text{LaAlO}_3/\text{SrTiO}_3$ heterointerface, *Nature (London)* **427**, 423 (2004).
- [2] E. Flekser, M. B. Shalom, M. Kim, C. Bell, Y. Hikita, H. Y. Hwang, and Y. Dagan, Magnetotransport effects in polar versus non-polar SrTiO_3 based heterostructures, *Phys. Rev. B* **86**, 121104(R) (2012).
- [3] R. Pentcheva and W. E. Pickett, Avoiding the polarization catastrophe in $\text{LaAlO}_3/\text{SrTiO}_3(001)$ through polar distortion, *Phys. Rev. Lett.* **102**, 107602 (2009).
- [4] M. B. Shalom, M. Sachs, D. Rakhmilevitch, A. Palevski, and Y. Dagan, Tuning spin-orbit coupling and superconductivity at the $\text{SrTiO}_3/\text{LaAlO}_3$ interface: a magnetotransport study, *Phys. Rev. Lett.* **104**, 126802 (2010).
- [5] G. Scheerer, M. Boselli, D. Pulmannova, C. W. Rischau, A. Waelchli, S. Gariglio, E. Giannini, D. van der Marel, and J.-M. Triscone, Ferroelectricity, superconductivity, and SrTiO_3 —passions of K.A. Müller, *Condens. Matter* **5**, 60 (2020).
- [6] M. Breitschaft, V. Tinkl, N. Pavlenko, S. Paetel, C. Richter, J. R. Kirtley, Y. C. Liao, G. Hammerl, V. Eyert, T. Kopp, and J. Mannhart, Two-dimensional electron liquid state at LaAlO_3 - SrTiO_3 interfaces, *Phys. Rev. B* **81**, 153414 (2010).
- [7] S. Davis, Z. Huang, K. Han, Ariando, T. Venkatesan, and V. Chandrasekhar, Magnetoresistance in the superconducting state at the (111) $\text{LaAlO}_3/\text{SrTiO}_3$ interface, *Phys. Rev. B* **96**, 134502 (2017).
- [8] Z. S. Popovic, S. Satpathy, and R. M. Martin, Origin of the two-dimensional electron gas carrier density at the LaAlO_3 on SrTiO_3 interface, *Phys. Rev. Lett.* **101**, 256801 (2008).
- [9] A. D. Caviglia, S. Gariglio, N. Reyren, D. Jaccard, T. Schneider, M. Gabay, S. Thiel, G. Hammerl, J. Mannhart, and J.-M. Triscone, Electric field control of the $\text{LaAlO}_3/\text{SrTiO}_3$ interface ground state, *Nature (London)* **456**, 624 (2008).
- [10] J. Biscaras, N. Bergeal, S. Hurand, C. Grossetete, A. Rastogi, R. C. Budhani, D. LeBoeuf, C. Proust, and J. Lesueur, Two-dimensional superconducting phase in $\text{LaTiO}_3/\text{SrTiO}_3$ heterostructures induced by high-mobility carrier doping, *Phys. Rev. Lett.* **108**, 247004 (2012).
- [11] N. Reyren, S. Thiel, A. D. Caviglia, L. F. Kourkoutis, G. Hammerl, C. Richter, C. W. Schneider, T. Kopp, A.-S. Ruetschi, D. Jaccard, M. Gabay, D. A. Muller, J.-M. Triscone, and J. Mannhart, Superconducting interfaces between insulating oxides, *Science* **317**, 1196 (2007).
- [12] J. A. Bert, K. C. Nowack, B. Kalisky, H. Noad, J. R. Kirtley, C. Bell, H. K. Sato, M. Hosoda, Y. Hikita, H. Y. Hwang, and K. A. Moler, Gate-tuned superfluid density at the superconducting $\text{LaAlO}_3/\text{SrTiO}_3$ interface, *Phys. Rev. B* **86**, 060503(R) (2012).
- [13] H. Nakamura and T. Kimura, Electric field tuning of spin-orbit coupling in KTaO_3 field-effect transistors, *Phys. Rev. B* **80**, 121308(R) (2009).
- [14] C. Liu, X. Yan, D. Jin, Y. Ma, H. W. Hsiao, Y. Lin, T. M. Bretz-Sullivan, X. Zhou, J. Pearson, B. Fisher, J. S. Jiang, W. Han, J. M. Zuo, J. Wen, D. D. Fong, J. Sun, H. Zhou, and A. Bhattacharya, Two-dimensional superconductivity and anisotropic transport at $\text{KTaO}_3(111)$ interfaces, *Science* **371**, 716 (2021).
- [15] Z. Chen, Y. Liu, H. Zhang, Z. Liu, H. Tian, Y. Sun, M. Zhang, Y. Zhou, J. Sun, and Y. Xie, Electric field control of superconductivity at the $\text{LaAlO}_3/\text{KTaO}_3(111)$ interface, *Science* **372**, 721 (2021).
- [16] Z. Chen, Z. Liu, Y. Sun, X. Chen, Y. Liu, H. Zhang, H. Li, M. Zhang, S. Hong, T. Ren, C. Zhang, H. Tian, Y. Zhou, J. Sun, and Y. Xie, Two-dimensional superconductivity at the $\text{LaAlO}_3/\text{KTaO}_3(110)$ heterointerface, *Phys. Rev. Lett.* **126**, 026802 (2021).
- [17] Y. Ma, J. Niu, W. Xing, Y. Yao, R. Cai, J. Sun, X. C. Xie, X. Lin, and W. Han, Superconductor-metal quantum transition at the EuO/KTaO_3 interface, *Chin. Phys. Lett.* **37**, 117401 (2020).
- [18] K. Ueno, S. Nakamura, H. Shimotani, H. T. Yuan, N. Kimura, T. Nojima, H. Aoki, Y. Iwasa, and M. Kawasaki, Discovery of superconductivity in KTaO_3 by electrostatic carrier doping, *Nat. Nanotechnol.* **6**, 408 (2011).
- [19] X. Hua, F. Meng, Z. Huang, Z. Li, S. Wang, B. Ge, Z. Xiang, and X. Chen, Tunable two-dimensional superconductivity and spin-orbit coupling at the $\text{EuO}/\text{KTaO}_3(110)$ interface, *npj Quantum Mater.* **7**, 97 (2022).
- [20] C. Liu, X. Zhou, D. Hong, B. Fisher, H. Zheng, J. Pearson, D. Jin, M. R. Norman, and A. Bhattacharya, Tunable superconductivity at the oxide-insulator/ KTaO_3 interface and its origin, *Nat. Commun.* **14**, 951 (2023).
- [21] N. Nakagawa, H. Y. Hwang, and D. A. Muller, Why some interfaces cannot be sharp, *Nat. Mater.* **5**, 204 (2006).
- [22] D. A. Muller, N. Nakagawa, A. Ohtomo, J. L. Grazul, and H. Y. Hwang, Atomic-scale imaging of nanoengineered oxygen vacancy profiles in SrTiO_3 , *Nature (London)* **430**, 657 (2004).
- [23] P. R. Willmott, S. A. Pauli, R. Herger, C. M. Schlepütz, D. Martocchia, B. D. Patterson, B. Delley, R. Clarke, D. Kumah, C. Cionca, and Y. Yacoby, Structural basis for the conducting interface between LaAlO_3 and SrTiO_3 , *Phys. Rev. Lett.* **99**, 155502 (2007).
- [24] C. Bigi, P. Orgiani, J. Slawinska, J. Fujii, J. T. Irvine, S. Picozzi, G. Panaccione, I. Vobornik, G. Rossi, D. Payne, and F. Borgatti, Direct insight into the band structure of SrNbO_3 , *Phys. Rev. Mater.* **4**, 025006 (2020).
- [25] J. M. Ok, N. Mohanta, J. Zhang, S. Yoon, S. Okamoto, E. S. Choi, H. Zhou, M. Briggeman, P. Irvin, A. R. Lupini, Y.-Y. Pai, E. Skoropata, C. Sohn, H. Li, H. Miao, B. Lawrie, W. S. Choi, G. Eres, J. Levy, and H. N. Lee, Correlated oxide Dirac semimetal in the extreme quantum limit, *Sci. Adv.* **7**, eabf9631 (2021).
- [26] T. Zhang, Y. Jiang, Z. Song, H. Huang, Y. He, Z. Fang, H. Weng, and C. Fang, Catalogue of topological electronic materials, *Nature (London)* **566**, 475 (2019).
- [27] See Supplemental Material at <http://link.aps.org/supplemental/10.1103/PhysRevB.109.205404> for methods of sample preparations, transport measurements, density functional theory calculations, and discussions on strain gradient, magnetoresistance, Hall resistivity, effective mass, and spatial distribution of interfacial charge system. The Supplemental Material also contains Refs. [28–30].
- [28] G. Kresse and J. Furthmüller, Efficient iterative schemes for *ab initio* total-energy calculations using a plane-wave basis set, *Phys. Rev. B* **54**, 11169 (1996).
- [29] G. Kresse and D. Joubert, From ultrasoft pseudopotentials to the projector augmented-wave method, *Phys. Rev. B* **59**, 1758 (1999).
- [30] J. P. Perdew, K. Burke, and M. Ernzerhof, Generalized gradient approximation made simple, *Phys. Rev. Lett.* **77**, 3865 (1996).

- [31] J. H. You, J. H. Lee, S. Okamoto, V. Cooper, and H. N. Lee, Strain effects on the electronic properties in δ -doped oxide superlattices, *J. Phys. D: Appl. Phys.* **48**, 085303 (2015).
- [32] J. Zhang, J. M. Ok, Y.-Y. Pai, J. Lapano, E. Skoropata, A. R. Mazza, H. Li, A. Huon, S. Yoon, B. Lawrie, M. Brahlek, T. Z. Ward, G. Eres, H. Miao, and H. N. Lee, Extremely large magnetoresistance in high-mobility SrNbO₃/SrTiO₃ heterostructures, *Phys. Rev. B* **104**, L161404 (2021).
- [33] C. S. Koonce, M. L. Cohen, J. F. Schooley, W. R. Hosler, and E. R. Pfeiffer, Superconducting transition temperatures of semiconducting SrTiO₃, *Phys. Rev.* **163**, 380 (1967).
- [34] M. Thiemann, M. H. Beutel, M. Dressel, N. R. Lee-Hone, D. M. Broun, E. Fillis-Tsirakis, H. Boschker, J. Mannhart, and M. Scheffler, Single-gap superconductivity and dome of superfluid density in Nb-Doped SrTiO₃, *Phys. Rev. Lett.* **120**, 237002 (2018).
- [35] G. Binnig, A. Baratoff, H. E. Hoening, and J. G. Bednorz, Two-band superconductivity in Nb-Doped SrTiO₃, *Phys. Rev. Lett.* **45**, 1352 (1980).
- [36] C. Lin and A. A. Demkov, Electron correlation in oxygen vacancy in SrTiO₃, *Phys. Rev. Lett.* **111**, 217601 (2013).
- [37] Y. Kozuka, M. Kim, C. Bell, B. G. Kim, Y. Hikita, and H. Y. Hwang, Two-dimensional normal-state quantum oscillations in a superconducting heterostructure, *Nature (London)* **462**, 487 (2009).
- [38] A. D. Caviglia, S. Gariglio, C. Cancellieri, B. Sacepe, A. Fete, N. Reyren, M. Gabay, A. F. Morpurgo, and J.-M. Triscone, Two-dimensional quantum oscillations of the conductance at LaAlO₃/SrTiO₃ interfaces, *Phys. Rev. Lett.* **105**, 236802 (2010).
- [39] B. Jalan, S. Stemmer, S. Mack, and S. J. Allen, Two-dimensional electron gas in δ -doped SrTiO₃, *Phys. Rev. B* **82**, 081103(R) (2010).
- [40] M. Ben Shalom, A. Ron, A. Palevski, and Y. Dagan, Shubnikov–De Haas oscillations in SrTiO₃/LaAlO₃ interface, *Phys. Rev. Lett.* **105**, 206401 (2010).
- [41] Y. Xie, C. Bell, M. Kim, H. Inoue, Y. Hikita, and H. Y. Hwang, Quantum longitudinal and Hall transport at the LaAlO₃/SrTiO₃ interface at low electron densities, *Solid State Commun.* **197**, 25 (2014).
- [42] G. Cheng, A. Annadi, S. Lu, H. Lee, J.-W. Lee, M. Huang, C.-B. Eom, P. Irvin, and J. Levy, Shubnikov–de Haas–like quantum oscillations in artificial one-dimensional LaAlO₃/SrTiO₃ electron channels, *Phys. Rev. Lett.* **120**, 076801 (2018).
- [43] X. Lin, G. Bridoux, A. Gourgout, G. Seyfarth, S. Krämer, M. Nardone, B. Fauqué, and K. Behnia, Critical doping for the onset of a two-band superconducting ground state in SrTiO_{3- δ} , *Phys. Rev. Lett.* **112**, 207002 (2014).
- [44] M. N. Gastiasoro, J. Ruhman, and R. M. Fernandes, Superconductivity in dilute SrTiO₃ : A review, *Ann. Phys.* **417**, 168107 (2020).